The Astronomical Journal, 141:145 (10pp), 2011 May doi:10.1088/0004-6256/141/5/145

NEW PRECISION ORBITS OF BRIGHT DOUBLE-LINED SPECTROSCOPIC BINARIES. VI. HD 24623 AND V923 SCORPII

Francis C. Fekel[1], Michael H. Williamson, and Gregory W. Henry
Center of Excellence in Information Systems, Tennessee State University, 3500 John A. Merritt Boulevard, Box 9501, Nashville, TN 37209, USA;
fekel@evans.tsuniv.edu, michael.h.williamson@gmail.com, gregory.w.henry@gmail.com
Received 2010 December 17; accepted 2011 January 19; published 2011 March 28

ABSTRACT

Using new radial velocities obtained at KPNO and Fairborn Observatory, we have determined improved spectroscopic orbits for two double-lined F-type binaries, HD 24623 and V923 Sco. The orbital periods are 19.66304 and 34.8386 days, respectively, so it is not surprising that their orbits have relatively high eccentricities of nearly 0.5. The orbital dimensions ($a_1 \sin i$ and $a_2 \sin i$) and minimum masses ($m_1 \sin^3 i$ and $m_2 \sin^3 i$) have accuracies of 0.2% or better. Extensive photometry of HD 24623 with the T4 0.75 m automatic photometric telescope at Fairborn Observatory shows no evidence of eclipses. Instead, a very weak reflection effect is seen, making the system a new variable star. Our spectroscopic ephemeris for V923 Sco indicates that the eclipse detected by Bolton and Herbst is a partial eclipse of the primary but detection of the secondary eclipse is uncertain. For HD 24623, we have determined spectral types of F2 dwarf and F4 dwarf for the primary and secondary, respectively. Our spectral types are F4 dwarf for the two components of V923 Sco. Both components of HD 24623 are rotating more slowly than their pseudosynchronous velocities, as is the primary of V923 Sco. However, the secondary of V923 Sco is likely rotating pseudosynchronously.

Key words: binaries: eclipsing – binaries: spectroscopic – stars: individual (HD 24623, V923 Sco) – stars: variables: general

1. INTRODUCTION

The overlap of the spectroscopic and visual binary domains has greatly increased over the past two decades with the advent of improvements in optical and near-infrared interferometry (Quirrenbach 2001). This bodes well for an expansion of the fundamental stellar database because precise masses and parallaxes can be obtained from the three-dimensional orbits of binary stars that are resolved as both a spectroscopic and a visual binary. Cunha et al. (2007) provided a list of over 30 interferometric visual orbits for double-lined spectroscopic binaries, while Torres et al. (2010) identified 23 interferometric systems with stellar masses determined to better than 3%. In addition, work on individual systems (e.g., Hummel et al. 2001; Boden et al. 2006; Fekel et al. 2009a) has led to useful comparisons with evolutionary theory.

In SB9, the continually updated web-based edition of the spectroscopic binary orbit catalog (Pourbaix et al. 2004), many of the older spectroscopic orbits have been computed with radial velocities from photographic plates. Because the photographic plates generally have lower resolutions and lower signal-to-noise ratios than modern CCD observations, results from them limit the precision of three-dimensional orbits. Thus, in previous papers of this series (Tomkin & Fekel 2006, 2008; Fekel et al. 2009b, 2010; Fekel & Williamson 2010), we have obtained new radial velocities and computed new spectroscopic orbits for bright field spectroscopic binaries, which are the most accessible systems to interferometry. These improved spectroscopic orbits will greatly enhance prospective interferometric observations of these systems.

In this paper, we use new velocities to compute orbits for two F-type systems, HD 24623 and V923 Sco. With our updated ephemeris, we search our extensive photometric observations of HD 24623 for eclipses. We provide an improved ephemeris for V923 Sco, which we compare with the limited photometric eclipse observations of Bolton & Herbst (1976). We discuss the evolutionary status of the two systems and the properties of their components. Table 1 lists some basic information from the literature for the two binary systems.

2. BRIEF HISTORY

2.1. HD 24623 = HIP 18277

HD 24623 ($\alpha = 03^h54^m34^s.96$, $\delta = -09°31'13''.3$ (2000), $V = 7.06$) has been included in several extensive surveys. Eggen (1985) listed it as a suspected member of his Sirius Supercluster (Eggen 1984), although one of the criteria for membership, its radial velocity, was unknown. Olsen (1994) obtained Strömgren photometry of HD 24623 as part of a large survey of F- and G-type stars. Nordström et al. (1997) complemented the photometric survey with a spectroscopic one that included observations of nearly 600 early-F-type dwarfs. They found HD 24623 to be a double-lined spectroscopic binary with an orbital period of 19.6623 days and an eccentricity of 0.49. From objective prism plates, Houk & Swift (1999) classified the composite spectrum of HD 24623 as F0 V.

Since 1993, we have been using HD 24623 as a comparison star for long-term photometric observations of 40 Eri A. In 1996, we acquired complementary spectroscopic observations of HD 24623 and independently discovered its duplicity. We have continued the spectroscopic observations to obtain improved properties of the system.

2.2. V923 Sco = HR 6327 = HD 153890

In the course of routine radial velocity programs carried out at Radcliffe Observatory, South Africa, Bennett et al. (1963) discovered HR 6327 ($\alpha = 17^h03^m50^s.94$, $\delta = -38°09'09''.3$ (2000),

[1] Visiting Astronomer, Kitt Peak National Observatory, National Optical Astronomy Observatory, operated by the Association of Universities for Research in Astronomy, Inc., under cooperative agreement with the National Science Foundation.

Table 1
Basic Properties of the Program Stars

Name	HR	HD	Spectral Type	V[a] (mag)	$B-V$[a] (mag)	Parallax[b] (mas)	Period (days)
...	...	24623	F0V	7.06	0.365	7.51	19.66
V923 Sco	6327	153890	F3V	5.91	0.409	15.46	34.84

Notes.
[a] Perryman et al. (1997).
[b] van Leeuwen (2007).

$V = 5.91$) to be a double-lined spectroscopic binary and determined an orbit with a period of 34.8189 days. They estimated spectral types of F3 IV–V and F3 V for the components, while Malaroda (1975) and Houk (1982) both classified the combined spectrum as F3 V.

Because this relatively bright star is in the field of the open cluster NGC 6281, Feinstein & Forte (1974) obtained photometry of it but concluded that it is a non-member. Bolton & Herbst (1976) used HR 6327 as a comparison star, when they obtained photometric observations of the X-ray source HD 153919. During those observations, they observed a portion of an eclipse of HR 6327. Hammerschlag-Hensberge & Zuiderwijk (1977) also observed HR 6327 as a comparison star for photometry of HD 153919. Because of the eclipse found by Bolton & Herbst (1976), Kholopov et al. (1981) assigned HR 6327 the variable star name V923 Sco, which we use to identify it in the rest of this paper.

3. OBSERVATIONS AND REDUCTIONS

3.1. Spectroscopic

Our spectroscopic observations were collected at two observatories. From 1996 through 2010, we obtained nearly two dozen spectrograms of HD 24623 at KPNO with the coudé feed telescope and coudé spectrograph. The vast majority of those observations were made with a TI CCD detector, are centered at 6430 Å, cover a wavelength range of 84 Å, and have a resolution of 0.21 Å or a resolving power of just over 30,000. One additional spectrum was acquired of the lithium region at 6700 Å. Because the TI CCD was retired in the summer of 2010, a different CCD detector was used in 2010 September. Made by Semiconductor Technology Associates, the chip, called STA2, is a 2600 × 4000 array of 12 μpixels. The same spectrograph configuration as that used for our TI CCD spectra results in a wavelength range of 336 Å with the STA2 detector. Our observations with that CCD were centered at 6430 Å, and the spectrograph slit was set so that it produced a resolution of 0.21 Å, the same as that for our TI CCD spectra.

Our KPNO observations of V923 Sco were much less numerous. In 2010 April, we obtained just two double-lined spectra at 6430 Å with the coudé feed telescope, spectrograph, and TI CCD detector. Further details about the coudé observations and their data reduction are given in Tomkin & Fekel (2006).

From 2004 through 2010, we acquired an extensive number of observations of both systems with the Tennessee State University 2 m automatic spectroscopic telescope (AST), a fiber-fed echelle spectrograph, and a 2048 × 4096 SITe ST-002A CCD. The echelle spectrograms have 21 orders that cover the wavelength range 4920–7100 Å with an average resolution of 0.17 Å. The typical signal-to-noise ratio of these observations is ~80. Eaton & Williamson (2004, 2007) have given a more extensive description of the telescope and spectrograph, operated at Fairborn Observatory near Washington Camp in the Patagonia Mountains of southeastern Arizona.

The procedures used to measure the KPNO radial velocities have been described extensively in Tomkin & Fekel (2006). Here we note that the KPNO velocities were determined by cross-correlation with respect to IAU radial velocity standard stars that have similar spectral types to the program stars. The velocities adopted for those standards are from Scarfe (2010).

Fekel et al. (2009b) provided an extensive general description of velocity measurement of the Fairborn AST spectra. For both systems, we used a line list that consists mostly of Fe I lines. The resulting Fairborn velocities are absolute velocities. Our unpublished velocities of several IAU solar-type standard stars indicate that the Fairborn Observatory velocities have a small zero-point offset of −0.3 km s^{-1} relative to the velocities of Scarfe (2010). Thus, we have added 0.3 km s^{-1} to each Fairborn velocity.

3.2. Photometric

We have used HD 24623 as one of the three comparison stars for 40 Eri A, a target star in our long-term program to search for luminosity cycles in solar-type stars (see, e.g., Baliunas et al. 1998; Henry 1999; Hall et al. 2007, 2009). As a result, for HD 24623 we have collected 18 consecutive observing seasons of Strömgren b and y photometry with the T4 0.75 m automatic photometric telescope (APT) at Fairborn Observatory.

The T4 0.75 m APT is equipped with a single-channel precision photometer that uses a temperature-stabilized EMI 9124QB bi-alkali photomultiplier tube to measure photon count rates sequentially through Strömgren b and y filters. In normal operation, the APT observes each target star (D) in a quartet sequence with three ostensibly constant comparison stars (A, B, and C). From these measurements, we compute Strömgren b and y differential magnitudes for each of the six combinations of the four stars: D–A, D–B, D–C, C–A, C–B, and B–A. We then correct the Strömgren b and y differential magnitudes for differential extinction with nightly extinction coefficients and transform them to the Strömgren photometric system with yearly mean transformation coefficients. Finally, we combine the Strömgren b and y differential magnitudes into a single $(b+y)/2$ passband to improve the precision of the observations. Typical precision for a single measurement is ~0.0015 mag. Henry (1999) presents a detailed description of the observing techniques and data reduction procedures employed for these observations.

In this paper, we will analyze the B–A differential magnitudes from the 40 Eri A sequence, where star B is HD 24623 ($V = 7.06$, $B-V = 0.365$, F0) and star A is the comparison star HD 24833 ($V = 6.56$, $B-V = 0.498$, F5). During the 18 observing seasons between 1993 September and 2010 December, the T4 APT acquired one or two measurements of the 40 Eri A sequence during each clear night for a total of 1225 measurements. We found that the seasonal mean B–A differential magnitudes varied slightly from year to year over a total range of 0.0015 mag. We, therefore, normalized the differential magnitudes such that all seasonal means were equal to the mean of the first season. This minimizes the possible low-level effects of long-term variability in either star as well as small data calibration errors over the nearly two decades of observation. The standard deviation of the normalized B–A differential magnitudes from their mean is 0.0020 mag, slightly

Table 2
Radial Velocities of HD 24623

Hel. Julian Date (HJD −2,400,000)	Phase	V_1 (km s^{-1})	$(O-C)_1$ (km s^{-1})	Wt_1	V_2 (km s^{-1})	$(O-C)_2$ (km s^{-1})	Wt_2	Source[a]
50,363.934	0.267	−6.9	0.4	0.5	25.9	−0.6	1.0	KPNO
50,364.886	0.316	2.7	0.0	0.5	15.9	−0.4	1.0	KPNO
50,365.920	0.368	12.4	0.3	0.5	6.7	−0.1	1.0	KPNO
50,400.882	0.146	−41.6	0.5	0.5	61.7	−0.2	1.0	KPNO
50,401.808	0.194	−26.2	0.3	0.5	45.9	−0.1	1.0	KPNO
50,720.998	0.427	20.9	0.0	0.5	−2.2	0.1	1.0	KPNO
50,755.928	0.203	−23.7	0.0	0.5	43.1	−0.1	1.0	KPNO
50,756.945	0.255	−10.2	0.0	0.5	29.1	−0.4	1.0	KPNO
50,757.920	0.304	−0.2	−0.7	0.5	18.3	−0.2	1.0	KPNO
50,829.761	0.958	−3.2	0.0	0.5	21.8	−0.5	1.0	KPNO
53,022.687	0.483	28.7	0.2	0.8	−10.1	−0.2	0.9	Fair
53,023.687	0.534	34.3	−0.2	0.8	−16.0	0.1	0.9	Fair
53,053.594	0.055	−73.9	0.0	0.8	93.6	−0.8	0.9	Fair
53,285.946	0.872	45.9	−0.4	0.8	−28.1	0.0	0.9	Fair
53,291.925	0.176	−32.2	−0.2	0.8	52.0	0.3	0.9	Fair
53,296.935	0.431	21.0	−0.5	0.8	−2.8	0.0	0.9	Fair
53,302.920	0.735	51.7	−0.1	0.8	−33.6	0.1	0.9	Fair
53,309.995	0.095	−61.8	0.2	0.8	82.2	0.0	0.9	Fair
53,315.876	0.394	15.9	−0.2	0.8	2.5	−0.2	0.9	Fair
53,322.839	0.748	52.2	−0.1	0.8	−34.0	0.3	0.9	Fair
53,329.930	0.109	−56.8	−0.2	0.8	76.8	0.1	0.9	Fair
53,339.802	0.611	42.3	−0.1	0.8	−24.3	−0.1	0.9	Fair
53,350.865	0.173	−32.8	0.1	0.8	52.7	0.2	0.9	Fair
53,356.753	0.473	26.8	−0.3	0.8	−8.4	0.2	0.9	Fair
53,377.715	0.539	34.9	−0.1	0.8	−16.4	0.2	0.9	Fair
53,383.744	0.845	50.4	−0.1	0.8	−32.6	−0.2	0.9	Fair
53,390.738	0.201	−24.5	−0.2	0.8	43.9	0.1	0.9	Fair
53,401.763	0.762	52.8	0.0	0.8	−34.5	0.2	0.9	Fair
53,425.677	0.978	−26.6	−0.1	0.8	46.1	0.1	0.9	Fair
53,440.651	0.739	51.9	−0.1	0.8	−33.9	0.0	0.9	Fair
53,628.004	0.268	−7.8	−0.6	0.8	26.6	0.2	0.9	Fair
53,638.953	0.824	52.0	−0.3	0.5	−34.2	0.0	1.0	KPNO
53,639.946	0.875	45.3	−0.2	0.5	−27.4	−0.1	1.0	KPNO
53,641.017	0.929	21.6	−0.4	0.8	−3.2	0.1	0.9	Fair
53,653.977	0.589	40.3	0.0	0.8	−22.3	−0.3	0.9	Fair
53,666.935	0.248	−12.0	−0.1	0.8	31.4	0.2	0.9	Fair
53,679.887	0.906	35.4	0.3	0.8	−16.9	−0.2	0.9	Fair
53,692.859	0.566	38.0	0.0	0.8	−19.4	0.2	0.9	Fair
53,725.797	0.241	−14.3	−0.8	0.8	32.9	0.1	0.9	Fair
53,740.784	0.003	−55.4	−0.2	0.8	75.5	0.2	0.9	Fair
53,753.698	0.660	46.7	−0.1	0.8	−28.4	0.2	0.9	Fair
53,766.692	0.321	3.5	−0.2	0.8	15.6	0.3	0.9	Fair
53,779.658	0.980	−29.4	−0.1	0.8	48.9	0.0	0.9	Fair
53,793.688	0.694	49.2	−0.1	0.8	−31.0	0.2	0.9	Fair
54,027.949	0.608	41.9	−0.3	0.8	−23.9	0.0	0.9	Fair
54,040.904	0.266	−7.9	−0.4	0.8	26.8	0.1	0.9	Fair
54,066.837	0.585	39.8	−0.2	0.8	−21.6	0.1	0.9	Fair
54,080.816	0.296	−1.3	−0.2	0.8	19.9	−0.3	0.9	Fair
54,094.732	0.004	−55.8	0.1	0.8	75.9	−0.1	0.9	Fair
54,108.747	0.717	50.9	0.1	0.8	−32.6	0.1	0.9	Fair
54,126.638	0.627	43.3	−0.6	0.8	−25.6	0.1	0.9	Fair
54,367.964	0.900	38.0	0.1	0.5	−19.5	0.1	1.0	KPNO
54,408.819	0.977	−25.6	0.2	0.5	45.3	−0.1	1.0	KPNO
54,526.615	0.968	−14.9	−0.2	0.5	34.3	0.2	1.0	KPNO
54,911.627	0.549	35.7	−0.4	0.5	−17.9	−0.2	1.0	KPNO
54,912.604	0.598	41.2	−0.1	0.5	−23.1	−0.1	1.0	KPNO
55,093.948	0.821	52.2	−0.3	0.5	−34.5	−0.1	1.0	KPNO
55,094.957	0.872	46.3	0.1	0.5	−27.7	0.3	1.0	KPNO
55,258.658	0.198	−25.5	−0.2	0.8	44.8	0.0	0.9	Fair
55,276.617	0.111	−56.1	−0.4	0.8	76.2	0.4	0.9	Fair
55,401.957	0.485	28.8	0.1	0.8	−10.2	0.0	0.9	Fair
55,442.837	0.564	38.1	0.3	0.8	−19.3	0.2	0.9	Fair
55,443.882	0.617	43.3	0.2	0.8	−24.7	0.1	0.9	Fair
55,444.831	0.666	46.9	−0.3	0.8	−29.0	0.1	0.9	Fair

Table 2
(Continued)

Hel. Julian Date (HJD −2,400,000)	Phase	V_1 (km s^{-1})	$(O-C)_1$ (km s^{-1})	Wt_1	V_2 (km s^{-1})	$(O-C)_2$ (km s^{-1})	Wt_2	Source[a]
55,445.833	0.717	50.6	−0.2	0.8	−32.1	0.6	0.9	Fair
55,449.837	0.920	28.1	0.2	0.8	−9.1	0.2	0.9	Fair
55,450.874	0.973	−20.6	−0.1	0.8	40.2	0.2	0.9	Fair
55,451.881	0.024	−70.3	−0.1	0.8	90.7	0.1	0.9	Fair
55,453.843	0.124	−51.1	−0.6	0.8	70.6	0.1	0.9	Fair
55,454.844	0.175	−32.5	−0.2	0.8	52.0	0.0	0.9	Fair
55,455.844	0.226	−17.6	−0.2	0.8	37.1	0.3	0.9	Fair
55,456.845	0.277	−5.6	−0.4	0.8	24.5	0.1	0.9	Fair
55,459.888	0.431	21.8	0.2	0.8	−2.3	0.7	0.9	Fair
55,463.784	0.630	44.2	0.0	0.8	−26.1	−0.1	0.9	Fair
55,463.978	0.639	44.9	−0.2	0.5	−27.0	−0.1	1.0	KPNO
55,464.836	0.683	48.2	−0.4	0.8	−30.3	0.1	0.9	Fair
55,464.931	0.688	48.8	−0.1	0.5	−31.0	−0.2	1.0	KPNO
55,465.836	0.734	51.8	0.1	0.8	−33.4	0.2	0.9	Fair
55,468.776	0.883	43.4	0.0	0.8	−25.0	0.1	0.9	Fair
55,470.783	0.986	−35.5	0.2	0.8	56.0	0.6	0.9	Fair
55,485.915	0.755	52.7	0.1	0.8	−34.1	0.4	0.9	Fair
55,490.761	0.002	−53.8	−0.2	0.8	73.8	0.2	0.9	Fair
55,491.766	0.053	−74.7	−0.5	0.8	94.7	0.0	0.9	Fair
55,492.730	0.102	−58.9	0.4	0.8	79.9	0.5	0.9	Fair
55,493.720	0.152	−40.2	−0.1	0.8	60.1	0.2	0.9	Fair
55,494.781	0.206	−22.7	0.1	0.8	42.7	0.4	0.9	Fair
55,502.876	0.618	43.4	0.3	0.8	−24.4	0.5	0.9	Fair
55,506.755	0.815	52.8	0.1	0.8	−34.4	0.3	0.9	Fair
55,508.926	0.925	24.8	0.1	0.8	−5.8	0.3	0.9	Fair
55,509.927	0.976	−24.1	0.4	0.8	44.3	0.3	0.9	Fair
55,511.891	0.076	−68.5	0.2	0.8	89.4	0.4	0.9	Fair
55,513.891	0.178	−31.2	0.2	0.8	50.9	−0.1	0.9	Fair
55,525.626	0.775	52.9	−0.2	0.8	−35.4	−0.4	0.9	Fair
55,526.626	0.826	52.5	0.3	0.8	−33.9	0.2	0.9	Fair
55,527.626	0.876	45.2	0.0	0.8	−27.1	−0.1	0.9	Fair
55,528.626	0.927	23.5	0.0	0.8	−4.5	0.3	0.9	Fair
55,529.726	0.983	−32.8	0.1	0.8	52.5	0.0	0.9	Fair
55,531.626	0.080	−67.4	0.0	0.8	87.9	0.2	0.9	Fair
55,532.646	0.132	−47.7	−0.1	0.8	67.4	−0.1	0.9	Fair
55,533.646	0.183	−29.6	0.3	0.8	49.5	0.0	0.9	Fair

Note. [a] KPNO: Kitt Peak National Observatory; Fair: Fairborn Observatory.

larger than the typical precision of 0.0015 mag cited above. This is because HD 24623 and its comparison star lie at a declination of −10° and so can never be observed from Fairborn through an air mass less than 1.3.

4. DETERMINATION OF ORBITS AND RESULTS

We have used several computer programs to determine the orbital elements. Preliminary orbits were computed with the program BISP (Wolfe et al. 1967), which implements a slightly modified version of the Wilsing–Russell method. Eccentric orbits were then determined with SB1 (Barker et al. 1967), a program that uses differential corrections. For a simultaneous solution of the two components we used SB2, which is a slightly modified version of SB1.

Reasons for the different velocity precisions of our various data sets have been discussed by Fekel et al. (2010). To combine the velocities into a single solution, we determined the weight for each set of our velocities, as well as those from the literature. We then computed the variances of the individual orbital solutions, which are inversely proportional to our adopted weights.

4.1. HD 24623

Between 1996 and 2010, we collected 21 KPNO and 79 Fairborn Observatory spectrograms that showed two sets of lines. After measuring the primary and secondary velocities (Table 2), we computed four independent single-lined orbital solutions and adopted weights of 1.0, 0.9, 0.8, and 0.5 for the KPNO secondary velocities, the AST secondary velocities, the AST primary velocities, and the KPNO primary velocities, respectively. The common elements of the individual solutions are generally in very good agreement. In particular, the center-of-mass velocities for the individual data sets differ by 0.3 km s^{-1} or less. Thus, we have combined the appropriately weighted velocities into a single solution, which has a period of 19.66304 days.

We next obtained individual solutions of the older literature velocities of Nordström et al. (1997). Adopting weights of 0.1 for their primary and secondary velocities, we included them with our new observations, obtaining a simultaneous orbital solution of the combined data. In that solution, the velocities of Nordström et al. (1997) are consistent with our orbit, but the uncertainties of the elements are not significantly improved, and so we adopt the orbit determined from just our new observations.

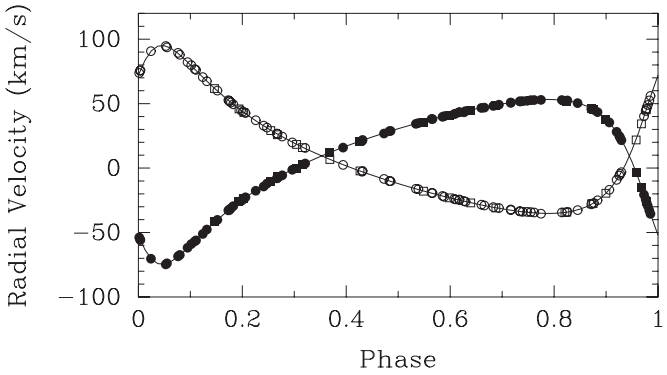

Figure 1. Radial velocities of HD 24623 compared with the computed velocity curves. Filled and open symbols represent the primary and secondary, respectively. Circles: Fairborn Observatory; squares: KPNO. Zero phase is a time of periastron passage.

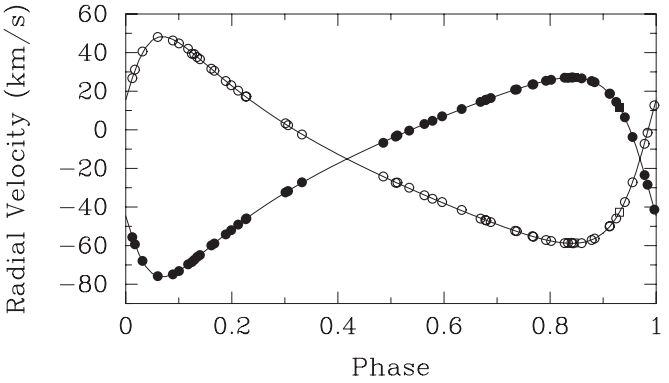

Figure 2. Radial velocities of V923 Sco compared with the computed velocity curves. Filled and open symbols represent the primary and secondary, respectively. Circles: Fairborn Observatory; squares: KPNO. Zero phase is a time of periastron passage.

Those elements are given in Table 3. Figure 1 compares our primary and secondary velocities with the calculated velocity curves. Zero phase is a time of periastron passage.

In addition to our new elements, Table 3 lists the orbital elements of Nordström et al. (1997). The two sets of elements, including the center-of-mass velocities, are in excellent agreement. Our new elements have a factor of ∼5 improvement in precision.

4.2. V923 Sco

Between 2004 and 2010, we obtained 56 spectra of V923 Sco at two observatories. Although V923 Sco can certainly be observed at KPNO, we acquired only two observations of it at that observatory because with a declination of −38° it rises just 20° above the horizon. Its short window of observability makes it poorly suited for our general KPNO observing strategy, which consists of three one-week observing runs per year. Fortunately, limited observing runs are not a problem with our 2 m AST at Fairborn Observatory, where we were able to obtain 54 spectra at double-lined phases. All our observations are listed in Table 4.

After measuring the primary and secondary velocities, we computed two independent single-lined orbital solutions, one for the primary and one for the secondary. Because the number of KPNO observations is so small, we simply included the velocities from that observatory in the two orbital solutions of the Fairborn velocities. Comparing the variances for the two solutions, we adopted weights of 1.0 and 0.3 for the primary and secondary components, respectively. Common elements of the two orbits are in excellent accord. A simultaneous solution of the appropriately weighted primary and secondary velocities resulted in a period of 34.8386 days.

In principle, the older literature velocities could be used to improve the precision of the orbital period because the observations of Bennett et al. (1963) began 460 cycles earlier than ours. However, the old velocities are from photographic plates that have significantly lower resolution than our observations. A joint solution of the primary velocities of Bennett et al. (1963), which were given weights of 0.01, and ours indicates that the older velocities are consistent with our orbit, but they do not improve the period or the other elements. Therefore, we have chosen to list in Table 5 our simultaneous solution of the primary and secondary that has been determined with the new velocities from KPNO and Fairborn Observatory. Figure 2 compares our primary and secondary velocities with the calculated velocity curves. Zero phase is a time of periastron passage.

Table 5 lists the orbital elements of Bennett et al. (1963) and those of our new solution. Bennett et al. (1963) chose to identify the fainter, less massive star as component I. For comparison with our results, we have switched their component identification. Their orbital elements did not include T, a time of periastron passage, so we have listed the value from the catalog of Batten et al. (1989). Also, we have converted their probable errors to standard deviations. Comparing the elements of the two solutions, we see that they are generally in reasonable accord. In particular, the values of the center-of-mass velocities are within 1σ, so there is no evidence of a third component in the system. However, the precision of the elements has been improved by a factor of ∼20.

5. SPECTRAL TYPES AND MAGNITUDE DIFFERENCE

Strassmeier & Fekel (1990) identified several luminosity-sensitive and temperature-sensitive line ratios in the 6430–6465 Å region. They employed those critical line ratios and the general appearance of the spectrum as spectral-type criteria. However, for stars that are hotter than early-G spectral class, the line ratios in that wavelength region have little sensitivity to luminosity. So instead, the luminosity class has been determined by computing the absolute visual magnitude with the *Hipparcos* parallax and comparing that magnitude to evolutionary tracks.

Spectra of our two binaries were compared with the spectra of a number of F stars primarily from the lists of Abt & Morrell (1995), Johnson & Morgan (1953), and Fekel (1997). The reference-star spectra were obtained at KPNO with the same telescope, spectrograph, and detector as our binary star spectra. To facilitate a comparison, various combinations of the reference-star spectra were rotationally broadened, shifted in radial velocity, appropriately weighted, and added together with a computer program developed by Huenemoerder & Barden (1984) and Barden (1985) in an attempt to reproduce the binary spectra.

5.1. HD 24623

Houk & Swift (1999) classified the combined spectrum of HD 24623 as F0 V from an objective prism plate. In our high-dispersion spectra, the components have similar line depths but the primary is a bit broader than the secondary. A combination of HR 5075 (F2 V: Abt & Morrell 1995; [Fe/H] = −0.04: Boesgaard & Tripicco 1986) for the primary and θ Cyg (F4 V: Slettebak 1955; mean [Fe/H] = 0.01: Taylor 2005) for the

Table 3
Orbital Elements and Related Parameters of HD 24623

Parameter	Nordström et al. (1997)	This Study
P (days)	19.66227 ± 0.00037	19.663042 ± 0.000014
T (HJD)	2,447,861.470 ± 0.014	2,452,934.5350 ± 0.0025
e	0.491 ± 0.002	0.48873 ± 0.00038
ω_1 (deg)	130.0 ± 0.3	130.183 ± 0.060
K_1 (km s^{-1})	63.92 ± 0.19	63.958 ± 0.048
K_2 (km s^{-1})	65.08 ± 0.22	65.149 ± 0.045
γ (km s^{-1})	9.47 ± 0.09	9.439 ± 0.018
$m_1 \sin^3 i$ ($M_\odot$)	...	1.4725 ± 0.0024
$m_2 \sin^3 i$ ($M_\odot$)	...	1.4456 ± 0.0024
$a_1 \sin i$ (10^6 km)	...	15.087 ± 0.012
$a_2 \sin i$ (10^6 km)	...	15.368 ± 0.011
Standard error of an observation of unit weight (km s^{-1})	...	0.3

secondary provides a good fit to the double-lined spectrum of HD 24623. Thus, the components have approximately solar iron abundances.

The continuum intensity ratio of the secondary/primary is 0.776, which results in a continuum magnitude difference of 0.28 at 6430 Å. The secondary has a similar spectral class to the primary, and so we adopt a V mag difference of 0.3. As discussed in Section 6.1, visual magnitudes from the reanalyzed *Hipparcos* parallax (van Leeuwen 2007) indicate that both components are on the main sequence.

5.2. V923 Sco

Malaroda (1975) and Houk (1982) both classified the combined spectrum of V923 Sco as F3 V, while Bennett et al. (1963) had earlier called the components F3 IV–V and F3 V and noted that the spectra "differ only slightly in character and intensity." Our high-dispersion spectra show that the components are indeed rather similar, although the secondary is a bit weaker and rotating somewhat faster than the primary. We found a good fit to both components of the composite spectrum with θ Cyg (F4 V: Slettebak 1955; mean [Fe/H] = 0.01: Taylor 2005). Thus, the two components have essentially solar iron abundances.

The continuum intensity ratio of the secondary/primary is 0.754, which results in a continuum magnitude difference of 0.31 at 6430 Å. The secondary has a similar spectral class to the primary, and so we adopt a V mag difference of 0.3. As discussed in Section 6.2, visual magnitudes from the reanalyzed *Hipparcos* parallax (van Leeuwen 2007) indicate that both components are on the main sequence.

6. BASIC PROPERTIES

6.1. HD 24623

For HD 24623, we begin by adopting a V mag of 7.06 and a $B - V$ color of 0.365 mag from the *Hipparcos* catalog (Perryman et al. 1997). With our magnitude difference of 0.3, the individual V magnitudes are 7.67 and 7.97 for the primary and secondary, respectively. The new *Hipparcos* parallax reduction by van Leeuwen (2007) produces a value of 7.51 ± 0.59 mas and corresponds to a distance of 133.2 ± 10.5 pc. Even though there may be a slight amount of reddening at this distance, we assume that it is negligible. The resulting absolute magnitudes are M_V = 2.0 ± 0.2 mag and M_V = 2.3 ± 0.2 mag for the primary and secondary, respectively. Guided by Johnson (1966), we assume $B - V$ colors of 0.35 for the primary and 0.38 for the secondary, which, when combined for the two stars, produce a $B - V$ color similar to the observed value. Then, from Table 3 of Flower (1996), we obtain the bolometric corrections and effective temperatures of the two components. Finally, with the use of the Stefan–Boltzmann law, the luminosities of the primary and secondary are $L_1 = 11.5 \pm 1.9\ L_\odot$ and $L_2 = 8.8 \pm 1.4\ L_\odot$, respectively, while the radii are $R_1 = 2.3 \pm 0.2\ R_\odot$ and $R_2 = 2.1 \pm 0.2\ R_\odot$, respectively. The uncertainties in the computed quantities are dominated by the parallax uncertainty and the effective temperature uncertainty with the latter estimated to be ± 200 K.

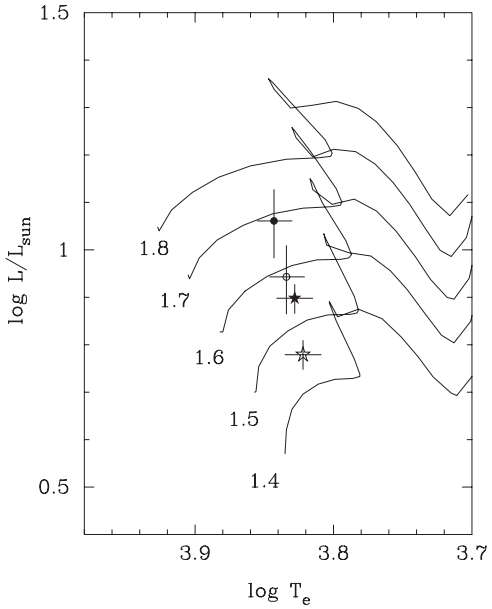

Figure 3. Positions of the components of HD 24623 (circles) and V923 Sco (stars) are compared with the 1.4–1.8 $M_\odot$ solar-abundance evolutionary tracks of Girardi et al. (2000) in a theoretical H-R diagram. The more massive component in each system corresponds to the filled symbol. Our estimated uncertainties are shown.

The estimated effective temperatures and derived luminosities of the components are compared with the solar-abundance evolutionary tracks of Girardi et al. (2000) in a theoretical H-R diagram (Figure 3). The primary to secondary mass ratio suggested by those results is about 1.06 compared with our derived value of 1.02. Adopting a smaller magnitude difference would improve the agreement.

6.2. V923 Sco

From the *Hipparcos* catalog (Perryman et al. 1997), we assume a V mag of 5.91 and a $B - V$ color of 0.409 mag for

Table 4
Radial Velocities of V923 Sco

Hel. Julian Date (HJD −2,400,000)	Phase	V_1 (km s^{-1})	$(O-C)_1$ (km s^{-1})	Wt_1	V_2 (km s^{-1})	$(O-C)_2$ (km s^{-1})	Wt_2	Source[a]
53,091.993	0.125	−68.5	−0.2	1.0	39.4	−0.7	0.3	Fair
53,432.998	0.913	18.8	0.2	1.0	−49.8	0.2	0.3	Fair
53,460.010	0.688	16.5	0.1	1.0	−47.8	0.0	0.3	Fair
53,472.975	0.060	−75.8	0.1	1.0	48.1	0.1	0.3	Fair
53,499.917	0.834	26.9	−0.2	1.0	−58.6	0.2	0.3	Fair
53,525.856	0.578	4.7	0.0	1.0	−35.7	−0.1	0.3	Fair
53,539.792	0.978	−23.4	−0.2	1.0	−7.2	−0.5	0.3	Fair
53,604.663	0.840	27.1	0.0	1.0	−58.5	0.3	0.3	Fair
53,846.859	0.792	25.4	0.0	1.0	−57.1	−0.1	0.3	Fair
53,859.918	0.167	−58.9	−0.1	1.0	30.6	0.3	0.3	Fair
53,877.784	0.680	15.7	0.1	1.0	−47.0	−0.1	0.3	Fair
53,896.817	0.226	−46.3	−0.1	1.0	17.2	0.0	0.3	Fair
54,889.991	0.734	20.8	0.0	1.0	−52.3	0.0	0.3	Fair
54,903.944	0.134	−65.9	0.2	1.0	37.7	−0.2	0.3	Fair
54,916.989	0.509	−3.5	−0.1	1.0	−27.4	−0.2	0.3	Fair
54,925.974	0.767	23.5	−0.1	1.0	−55.1	0.1	0.3	Fair
54,933.980	0.997	−41.3	0.1	1.0	12.7	0.5	0.3	Fair
54,938.973	0.140	−64.9	0.0	1.0	36.6	0.0	0.3	Fair
54,951.946	0.512	−2.9	0.1	1.0	−27.3	0.3	0.3	Fair
54,960.873	0.769	23.6	−0.1	1.0	−55.4	−0.1	0.3	Fair
54,962.925	0.827	27.0	0.1	1.0	−58.7	0.0	0.3	Fair
54,964.891	0.884	24.7	0.0	1.0	−56.3	0.0	0.3	Fair
54,975.861	0.199	−52.0	−0.2	1.0	23.1	0.1	0.3	Fair
54,985.849	0.485	−6.7	−0.4	1.0	−24.2	0.0	0.3	Fair
54,998.876	0.859	26.7	0.0	1.0	−58.7	−0.2	0.3	Fair
55,004.871	0.031	−67.9	0.1	1.0	40.6	0.8	0.3	Fair
55,031.714	0.802	25.9	0.0	1.0	−57.6	0.0	0.3	Fair
55,041.706	0.089	−74.9	−0.1	1.0	46.3	−0.6	0.3	Fair
55,042.707	0.117	−69.7	0.1	1.0	42.0	0.3	0.3	Fair
55,060.682	0.633	10.8	0.0	1.0	−41.5	0.4	0.3	Fair
55,245.022	0.925	14.5	0.1	1.0	−45.9	−0.3	0.3	Fair
55,255.028	0.212	−49.1	0.0	1.0	20.3	0.1	0.3	Fair
55,270.947	0.669	14.5	0.0	1.0	−46.0	−0.3	0.3	Fair
55,280.929	0.955	−3.7	−0.4	1.0	−27.2	0.1	0.3	Fair
55,281.915	0.984	−28.4	0.2	1.0	−1.5	−0.4	0.3	Fair
55,282.915	0.012	−55.6	−0.1	1.0	26.8	−0.1	0.3	Fair
55,285.979	0.100	−73.2	−0.1	1.0	44.8	−0.3	0.3	Fair
55,286.979	0.129	−67.4	−0.1	1.0	39.3	0.2	0.3	Fair
55,311.862	0.843	27.1	0.0	1.0	−58.8	0.0	0.3	Fair
55,311.937	0.845	27.1	0.0	1.0	−58.6	0.2	0.3	KPNO
55,314.917	0.931	11.8	0.2	1.0	−42.7	0.1	0.3	KPNO
55,317.928	0.017	−59.3	0.1	1.0	31.2	0.3	0.3	Fair
55,322.944	0.161	−59.9	0.2	1.0	31.7	0.1	0.3	Fair
55,327.814	0.301	−32.4	0.1	1.0	3.4	0.5	0.3	Fair
55,328.896	0.332	−27.2	0.2	1.0	−2.4	−0.1	0.3	Fair
55,336.936	0.563	3.0	0.1	1.0	−33.9	−0.1	0.3	Fair
55,358.732	0.189	−54.2	−0.2	1.0	25.3	0.0	0.3	Fair
55,362.825	0.306	−31.7	−0.1	1.0	2.4	0.3	0.3	Fair
55,370.781	0.534	−0.4	0.0	1.0	−30.0	0.3	0.3	Fair
55,375.780	0.678	15.4	0.0	1.0	−46.7	0.0	0.3	Fair
55,382.759	0.878	25.3	−0.1	1.0	−57.1	−0.1	0.3	Fair
55,412.681	0.737	20.9	−0.2	1.0	−52.5	0.1	0.3	Fair
55,442.619	0.596	7.0	0.3	1.0	−37.4	0.3	0.3	Fair
55,453.612	0.912	18.7	−0.2	1.0	−50.1	0.2	0.3	Fair
55,454.618	0.941	6.5	0.1	1.0	−37.4	−0.1	0.3	Fair
55,464.602	0.227	−45.9	0.0	1.0	17.3	0.4	0.3	Fair

Note. [a] Fair: Fairborn Observatory; KPNO: Kitt Peak National Observatory.

the V923 Sco composite system. With a component magnitude difference of 0.3, the individual V magnitudes are 6.52 and 6.82 for the primary and secondary, respectively. The new reduction of the *Hipparcos* parallax produces a value of 15.46 ± 0.40 mas (van Leeuwen 2007), which corresponds to a distance of 64.7 ± 1.7 pc. At such a distance, we assume that the system is not reddened, and so we obtain absolute magnitudes of M_v = 2.47 ± 0.08 and M_v = 2.77 ± 0.08 mag for the primary

Table 5
Orbital Elements and Related Parameters of V923 Sco

Parameter	Bennett et al. (1963)	This Study
P (days)	34.8189	34.838646 ± 0.000099
T (HJD)	2,430,028.332	2,454,272.1636 ± 0.0047
e	0.4234 ± 0.0116	0.47204 ± 0.00042
ω (deg)	107.13 ± 1.71	112.853 ± 0.074
K_1 (km s^{-1})	50.45 ± 0.83	51.652 ± 0.031
K_2 (km s^{-1})	53.63 ± 0.91	53.580 ± 0.054
γ (km s^{-1})	−14.83 ± 0.40	−15.078 ± 0.018
$m_1 \sin^3 i$ ($M_\odot$)	1.563	1.4708 ± 0.0031
$m_2 \sin^3 i$ ($M_\odot$)	1.470	1.4178 ± 0.0023
$a_1 \sin i$ (10^6 km)	21.89	21.814 ± 0.014
$a_2 \sin i$ (10^6 km)	23.27	22.629 ± 0.023
Standard error of a unit weight observation (km s^{-1})	...	0.15

and secondary, respectively. The small magnitude difference between the components indicates that they have similar colors, and so we only slightly adjust the $B - V$ colors to 0.399 for the primary and 0.419 for the secondary. We adopt bolometric corrections and effective temperatures from Table 3 of Flower (1996). Then, using the Stefan–Boltzmann law, we obtain luminosities of $L_1 = 7.9 \pm 0.5$ and $L_2 = 6.0 \pm 0.4$ $L_\odot$ and radii of $R_1 = 2.0 \pm 0.1$ and $R_2 = 1.9 \pm 0.1$ $R_\odot$ for the primary and secondary, respectively. The uncertainties in the computed quantities of the primary and secondary are dominated by the parallax and the effective temperature uncertainties with the latter estimated to be ±200 K for both components.

The estimated effective temperatures and derived luminosities of the components are compared with the solar-abundance evolutionary tracks of Girardi et al. (2000) in a theoretical H-R diagram (Figure 3). The primary to secondary mass ratio suggested by those results is about 1.07 compared with our derived value of 1.04. As with HD 24623, adopting a smaller magnitude difference would increase the agreement. From the evolutionary tracks, the theoretical mass of the V923 Sco primary is about 5% too large, while the theoretical mass of the secondary is in better agreement with its observed value. The analysis of an improved eclipse light curve of V923 Sco might result in a better comparison with theory.

7. ECLIPSE SEARCHES

7.1. HD 24623

Periodogram analysis, based on least-squares fitting of sine curves, of our Fairborn Observatory B–A differential magnitudes reveals low-amplitude variability in HD 24623 with a period of 19.663 ± 0.001 days, in precise agreement with the binary orbital period from this study (Table 3). Therefore, in Figure 4, we plot our 1225 photometric observations phased with our orbital period of 19.66304 days. Zero phase is a time of periastron passage (Table 3). Small filled circles are the 1225 individual differential measurements. Large circles are mean values of the observations within bins of 0.005 phase units. Given that the orbit is eccentric, primary eclipses would occur closer to periastron passage (zero phase) and so are more likely to occur than secondary eclipses. From our orbital elements, we predict primary mid-eclipse to occur at phase 0.9647 and secondary mid-eclipse at phase 0.2525. Neither eclipse is seen in our data. Instead, there is a very small increase in light (0.002–0.003 mag) near periastron that we ascribe to the reflection effect.

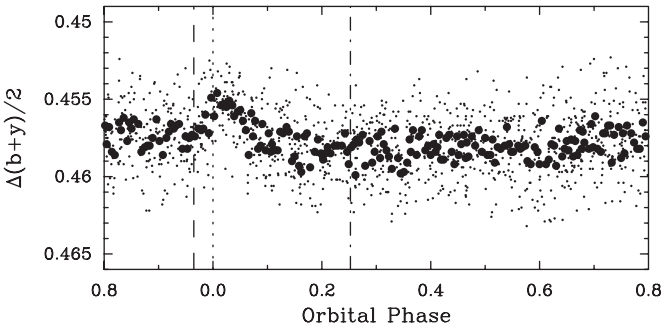

Figure 4. Differential magnitudes for HD 24623 phased with the orbital period of 19.66304 days, where zero phase (vertical dotted line) is a time of periastron passage. Small filled circles represent our 1225 individual observations; the large filled circles are the mean values of the observations within bins of 0.005 phase units. The vertical dashed line is the predicted phase of primary mid-eclipse, which is more likely to be detected because the components are nearer periastron. The vertical dash-dotted line is the predicted phase of secondary mid-eclipse. No eclipses are evident, but a very small light increase, which we ascribe to the reflection effect, occurs near periastron.

7.2. V923 Sco

With our significantly improved orbital elements, we obtain the following eclipse ephemerides. For mid-eclipse of the primary, which occurs closer to periastron,

$$T_{\rm conj}({\rm HJD}) = 2{,}454{,}271.4522(\pm 0.0047) + 34.83865(\pm 0.00010)E,$$

where E represents an integer number of cycles.

Figure 5 plots the photometry of Bolton & Herbst (1976), phased with our ephemeris for primary eclipse. Our phase of mid-eclipse also is indicated. From that comparison, we conclude that the eclipse ingress was almost completely observed and the primary eclipse is partial with a depth of ∼0.3 mag.

The ephemeris for mid-eclipse of the secondary is

$$T_{\rm conj}({\rm HJD}) = 2{,}454{,}284.3873(\pm 0.0047) + 34.83865(\pm 0.00010)E.$$

If phase 0.0 is adopted for mid-eclipse of the primary, as is generally done, then the predicted mid-eclipse of the secondary occurs at phase 0.3713.

Figure 6 shows the photometry of Bolton & Herbst (1976) near the time of predicted secondary eclipse. Because the orbit is eccentric, the orbital separation of the components at secondary eclipse is greater than that at primary eclipse.

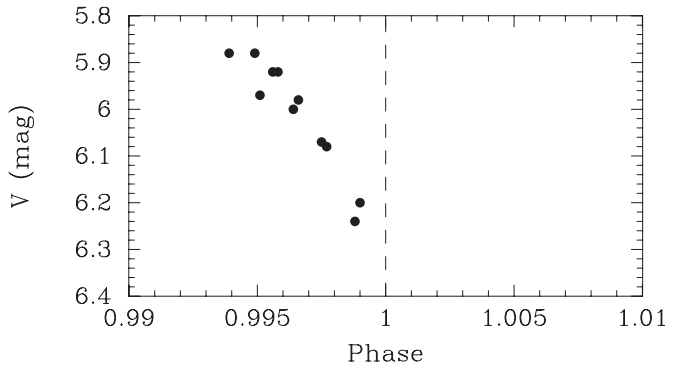

Figure 5. *V* mags of V923 Sco (Bolton & Herbst 1976) phased with our ephemeris for primary eclipse. The dashed line at phase 1.0 is our predicted mid-eclipse.

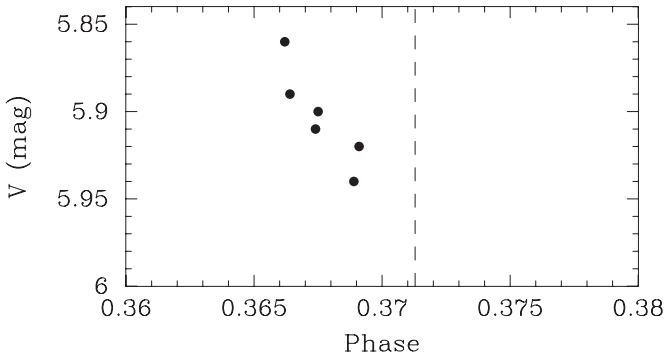

Figure 6. Phased *V* mags of V923 Sco (Bolton & Herbst 1976) near the time of secondary eclipse. The dashed line at phase 0.3713 indicates predicted mid-eclipse. The limited number of observations are suggestive of an eclipse but have a similar magnitude range to other observations that were obtained well outside of eclipse.

Although the observed phase coverage around secondary mid-eclipse is minimal, the individual observations near phase 0.37 suggest a light decrease at approximately the predicted time. The decrease is tantalizingly similar in character to that of the partially observed primary eclipse, suggesting the possibility that there is a detectable secondary eclipse. However, the *V* mag range of the drop just before phase 0.37 is very similar to the scatter in the out-of-eclipse photometry of Bolton & Herbst (1976). Thus, those observations do not provide a conclusive result, and additional precise photometry will be needed to determine if a secondary eclipse can be detected.

8. CIRCULARIZATION AND SYNCHRONIZATION

The two main theories of orbital circularization and rotational synchronization (e.g., Zahn 1977; Tassoul & Tassoul 1992) disagree significantly on absolute timescales but do agree that synchronization should occur first. Duquennoy & Mayor (1991) examined the multiplicity of solar-type stars in the solar neighborhood. They determined that systems with periods $\leqslant$10 days had circular orbits but that longer period orbits are generally eccentric. Both of our binaries have periods greater than 10 days, so it is not particularly surprising that these two systems have eccentric orbits.

In an eccentric orbit, Hut (1981) has shown that the rotational angular velocity of a star will tend to synchronize with that of the orbital motion at periastron. We compute the pseudosynchronous period with Equation (42) of Hut (1981).

To help in assessing pseudosynchronization in our two binaries, we have determined projected rotational velocities from our red-wavelength KPNO spectra with the procedure of Fekel (1997). For F-type stars, macroturbulent broadening has been taken into account. Following Fekel (1997), for early-F and mid-F stars values of 5 and 4 km s^{-1}, respectively, were adopted. To convert the v sin i values into equatorial rotational velocities, we assume, as is generally done, that the axes of the orbital and rotational planes are parallel, so the inclinations are equal.

8.1. HD 24623

To determine whether the components of HD 24623 are rotating pseudosynchronously, we compare our observed velocities with the predicted pseudosynchronous velocities. For HD 24623 our v sin i values, averaged from nine spectra, are 9.8 $\pm$ 1.0 and 5.9 $\pm$ 1.0 km s^{-1} for the primary and secondary, respectively. Nordström et al. (1997) estimated projected rotational velocities of 0 km s^{-1} for the two stars, suggesting that the rotational broadening in their spectra was unresolved.

The minimum masses of the two components are relatively large and similar. From our comparison with the solar-abundance evolutionary tracks of Girardi et al. (2000), we adopt a mass of 1.7 $M_{\odot}$ for the primary (Figure 3). Then that mass, combined with its m sin^3 i value (Table 3), results in an orbital inclination of 72°. If the rotational inclination is the same as that of the orbit, then the observed equatorial rotational velocities are 10 and 6 km s^{-1} for the primary and secondary, respectively. The pseudosynchronous rotation period of HD 24623 is 7.3 days. This value plus our computed radii from the Stefan–Boltzmann law produce pseudosynchronous rotational velocities of 16 and 14.5 km s^{-1} for the primary and secondary, respectively. Thus, the two components of HD 24623 are rotating roughly half as fast as their pseudosynchronous values.

8.2. V923 Sco

To determine whether the components of V923 Sco are pseudosynchronously rotating, we compute equatorial velocities from our projected rotational velocities and then compare them with the predicted pseudosynchronous velocities. For V923 Sco our v sin i values, averaged from two spectra, are 5.2 $\pm$ 1.0 and 8.0 $\pm$ 1.0 km s^{-1} for the primary and secondary, respectively. The system has partial eclipses, so its orbital inclination is very close to 90°. Thus, we adopt our v sin i values as the equatorial rotation velocities of the stars. Combining the pseudosynchronous rotation period (Hut 1981) of 13.6 days and our computed radii, we obtain pseudosynchronous rotational velocities of 7 km s^{-1} for both the primary and secondary. Comparison with the observed velocities indicates that the primary is rotating more slowly than its pseudosynchronous velocity, while the secondary is likely rotating pseudosynchronously.

9. CONCLUSIONS

We have determined improved double-lined orbits for HD 24623 and V923 Sco. Our extensive photometric observations of HD 24623 show no evidence for eclipses but do show a weak reflection effect at periastron. Our eclipse ephemerides confirm the primary eclipse found by Bolton & Herbst (1976) and indicate that it is partial. It is possible that part of a secondary eclipse was also detected by Bolton & Herbst (1976), but additional precise photometry will be necessary to confirm this.

For HD 24623, we have determined spectral types of F2 dwarf and F4 dwarf for the primary and secondary, respectively. Our spectral types are F4 dwarf for the two components of V923 Sco. Both components of HD 24623 are rotating more slowly than their pseudosynchronous velocities, as is the primary of V923 Sco. However, the secondary of V923 Sco is likely rotating pseudosynchronously.

From the revised *Hipparcos* parallaxes and adopted masses of the two systems, we have estimated the maximum angular separations of the components. The orbits of HD 24623 and V923 Sco are eccentric, and so we determined maximum nodal separations (e.g., McAlister 1976; Halbwachs 1981) of 1.7 and 4.4 mas, respectively. Although these separations are small, they are within the scope of modern optical interferometers. Thus, when our spectroscopic results are complemented with high-quality interferometric results, accurate three-dimensional orbits, masses, and distances for the systems will follow.

The help of Daryl Willmarth in support of the KPNO coudé feed observations is appreciated. The research at Tennessee State University has been supported in part by NASA, NSF, Tennessee State University, and the state of Tennessee through its Centers of Excellence program.

REFERENCES

Abt, H. A., & Morrell, N. I. 1995, ApJS, 99, 135
Baliunas, S. L., Donahue, R. A., Soon, W., & Henry, G. W. 1998, in ASP Conf. Ser. 154, The 10th Cambridge Workshop on Cool Stars, Stellar Systems, and the Sun, ed. R. A. Donahue & J. A. Bookbinder (San Francisco, CA: ASP), 153
Barden, S. C. 1985, ApJ, 295, 162
Barker, E. S., Evans, D. S., & Laing, J. D. 1967, R. Obs. Bull., 130, 355
Batten, A. H., Fletcher, J. M., & MacCarthy, D. G. 1989, Publ. Dom. Astrophys. Obs., 17, 1
Bennett, N. W. W., Evans, D. S., & Laing, J. D. 1963, R. Obs. Bull., 78, 391
Boden, A. F., Torres, G., & Latham, D. W. 2006, ApJ, 644, 1193
Boesgaard, A., & Tripicco, M. 1986, ApJ, 303, 724
Bolton, C. T., & Herbst, W. 1976, AJ, 81, 339
Cunha, M. S., et al. 2007, A&AR, 14, 217
Duquennoy, A., & Mayor, M. 1991, A&A, 248, 485
Eaton, J. A., & Williamson, M. H. 2004, Proc. SPIE, 5496, 710
Eaton, J. A., & Williamson, M. H. 2007, PASP, 119, 886
Eggen, O. J. 1984, AJ, 89, 1350
Eggen, O. J. 1985, PASP, 97, 807
Feinstein, A., & Forte, J. C. 1974, PASP, 86, 284
Fekel, F. C. 1997, PASP, 109, 514
Fekel, F. C., Boden, A. F., Tomkin, J., & Torres, G. 2009a, ApJ, 695, 1527
Fekel, F. C., Tomkin, J., & Williamson, M. H. 2009b, AJ, 137, 3900
Fekel, F. C., Tomkin, J., & Williamson, M. H. 2010, AJ, 139, 1579
Fekel, F. C., & Williamson, M. H. 2010, AJ, 140, 1381
Flower, P. J. 1996, ApJ, 469, 355
Girardi, L., Bressan, A., Bertelli, G., & Chiosi, C. 2000, A&AS, 141, 371
Halbwachs, J. L. 1981, A&AS, 44, 47
Hall, J. C., Henry, G. W., & Lockwood, G. W. 2007, AJ, 133, 2206
Hall, J. C., Henry, G. W., Lockwood, G. W., Skiff, B. A., & Saar, S. H. 2009, AJ, 138, 312
Hammerschlag-Hensberge, G., & Zuiderwijk, E. J. 1977, A&A, 54, 54
Henry, G. W. 1999, PASP, 111, 845
Houk, N. 1982, Michigan Catalogue of Two-dimensional Spectral Types for the HD Stars, Vol. 3 (Ann Arbor, MI: Univ. Michigan Press)
Houk, N., & Swift, C. 1999, Michigan Catalogue of Two-dimensional Spectral Types for the HD Stars, Vol. 5 (Ann Arbor, MI: Univ. Michigan Press)
Huenemoerder, D. P., & Barden, S. C. 1984, BAAS, 16, 510
Hummel, C. A., Carquillat, J.-M., Ginestet, N., Griffin, R. F., Boden, A. F., Hajian, A. R., Mozurkewich, D., & Nordgren, T. E. 2001, AJ, 121, 1623
Hut, P. 1981, A&A, 99, 126
Johnson, H. L. 1966, ARA&A, 4, 193
Johnson, H. L., & Morgan, W. W. 1953, ApJ, 117, 313
Kholopov, P. N., Samus, N. N., Kukarkina, N. P., Medvedeva, G. I., & Perova, N. B. 1981, IBVS, 1921
Malaroda, S. 1975, AJ, 80, 637
McAlister, H. A. 1976, PASP, 88, 317
Nordström, B., Stefanik, R. P., Latham, D. W., & Andersen, J. 1997, A&AS, 126, 21
Olsen, E. H. 1994, A&AS, 106, 257
Perryman, M. A. C., et al. 1997, A&A, 323, L49
Pourbaix, D., et al. 2004, A&A, 424, 727
Quirrenbach, A. 2001, ARA&A, 39, 353
Scarfe, C. D. 2010, Observatory, 130, 214
Slettebak, A. 1955, ApJ, 121, 653
Strassmeier, K. G., & Fekel, F. C. 1990, A&A, 230, 389
Tassoul, J.-L., & Tassoul, M. 1992, ApJ, 395, 259
Taylor, B. J. 2005, ApJS, 161, 444
Tomkin, J., & Fekel, F. C. 2006, AJ, 131, 2652
Tomkin, J., & Fekel, F. C. 2008, AJ, 135, 555
Torres, G., Andersen, J., & Giménez, A. 2010, A&AR, 18, 67
van Leeuwen, F. 2007, A&A, 474, 653
Wolfe, R. H., Horak, H. G., & Storer, N. W. 1967, in Modern Astrophysics, ed. M. Hack (New York: Gordon & Breach), 251
Zahn, J.-P. 1977, A&A, 57, 383